JOURNAL OF APPLIED POLYMER SCIENCE VOL. 21, 2791–2815 (1977)

The Tensile Fatigue Behavior of para-Oriented Aramid Fibers and Their Fracture Morphology

L. KONOPASEK and J. W. S. HEARLE, *Department of Textile Technology, University of Manchester Institute of Science and Technology, Manchester, England*

Synopsis

Samples of Fiber B and PRD 49 which were the forerunners of current Kevlar aramid fibers were subject to a limited number of tensile tests and tensile fatigue tests in order to determine their fracture morphology. The fibers were examined by optical and scanning electron microscopy. Both tensile and fatigue failure occurs by axial splitting, with the fatigue splits being much longer. Compressive effects in snap-back cause kink bands to form. The fatigue strength is only marginally less than the tensile strength.

INTRODUCTION

This paper describes studies of high-modulus aramid organic polymer fibers of a type which are now produced and sold by du Pont under the trade name Kevlar. These fibers are included in a type now known by the generic title aramid fibers.[1] When first introduced by du Pont, they were referred to as Fiber B and PRD 49: they are now given the trade name of Kevlar.

The types of Kevlar available are: Kevlar, intended for use in rubber tires, etc., and Kevlar-29, intended for use in high-strength textiles, both former Fiber B; and Kevlar-49, intended for use in rigid reinforced materials and other uses needing high stiffness, former PRD 49. The definition of an aramid fiber as given in the Textile Institute's "Textile Terms and Definitions," based on the U.S. Federal Trade Commission is: A fiber in which the fiber-forming substance is a long-chain synthetic polyamide in which at least 85% of the amide linkages are attached directly to two aromatic rings.

Two forms of Fiber B are believed to be the same in fiber constitution but different in finish; PRD 49 is a higher-stiffness version of the material. The samples tested were presumably typical of production some time ago, possibly on an experimental plant, but it must be realized that in a developing technology of this type, the structure of fibers supplied may be changed from time to time—either intentionally or otherwise. Lack of experience may also have led to fiber damage in handling. The constitution and method of manufacture of these fibers have not been disclosed, though statements by authors from other companies have appeared in the literature.[2,3] Their chemical structure is presumed to

consist of para-oriented benzene rings linked by —CONH— groups; Black and Preston[2] quote the following formulae:

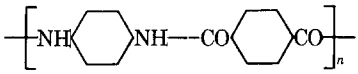

or

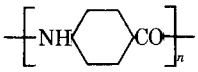

Meredith[4] states that Kevlar is poly(*p*-phenyleneterephthalamide), which is the first of the two formulae above.

Molecules of this type will be relatively stiff and strongly interactive with one

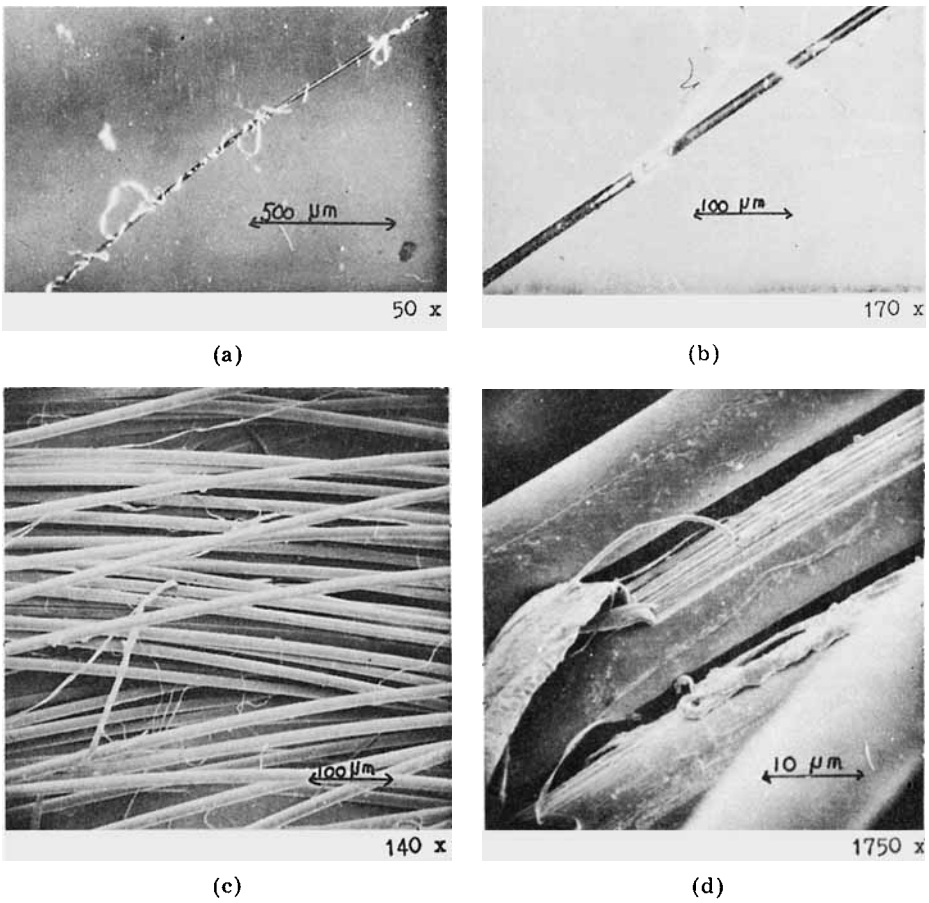

Fig. 1. SEM and optical microscope views of untested Fiber B and PRD 49 surface: (a), (b) Optical microscope views of Fiber B filaments as received at different magnifications. Note detached ribbon-like fibrillar layer separated from the filament and wound around it. (c), (d) SEM general views of Fiber B filaments as received at different magnification, showing many fibrils and fibrillar strands separated from the surface of the filaments. Note a "peeling" effect in (d). (e) Optical micrograph revealing the dark lines in Fiber B filaments, as seen in polarized light. (f), (g) SEM micrographs showing longitudinal splits and slightly bulging lines around the surface, in Fiber B and PRD 49, respectively.

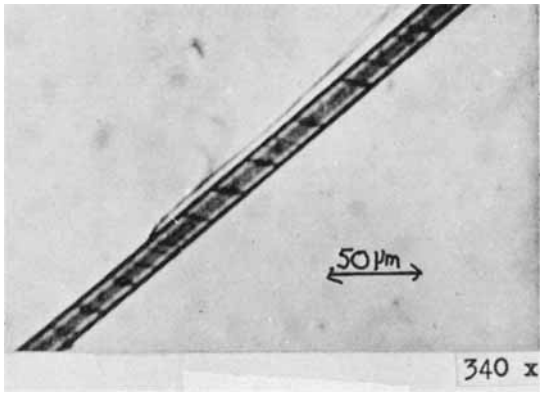

(e)

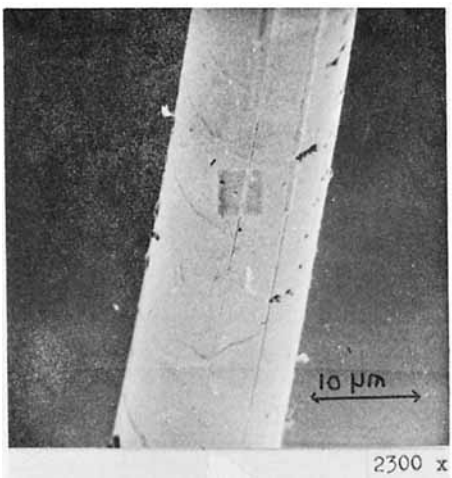

(f)

(g)

Fig. 1. (*continued from previous page*)

another. This, with the method of manufacture, leads to highly oriented fibers, with very high modulus, tenacity, and thermal stability. Several papers and bulletins describing their applications have appeared.[5,6]

The emphasis in the present work has been on a study of the tensile fatigue of these fibers using the fatigue tester developed by Bunsell et al.[7] and on the morphology of their fracture.

PRELIMINARY STUDIES

Fibers Examined

Two types of high-modulus, wholly aromatic polyamide fibers, designated as Fiber B and PRD 49, were obtained from du Pont in the form of multifilament yarns. The diameter of single filaments of both samples was found by optical microscopy to be approximately 12.4 μm. The linear density of single filaments was calculated to be 0.18 tex (1.61 den), by taking the density to be 1.44 g/cm^3 and assuming a circular cross section of filaments.

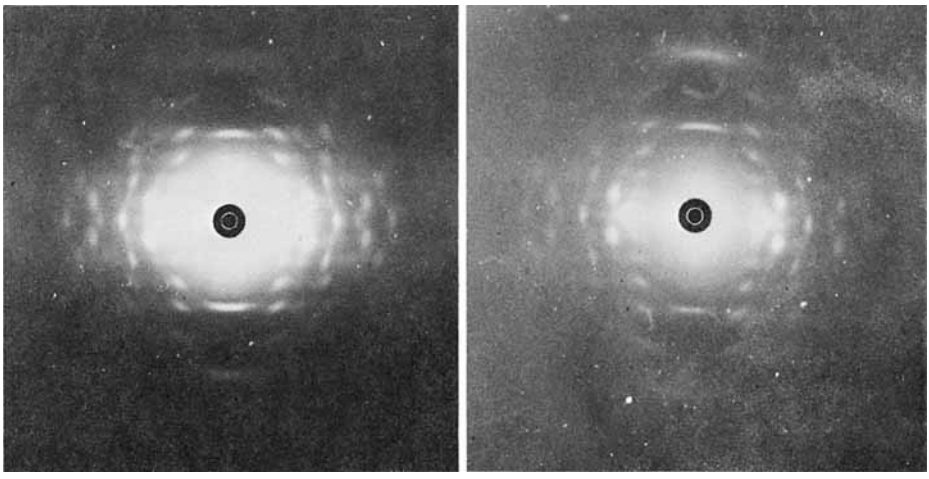

(a) (b)

Fig. 2. X-ray diffraction pictures of Fiber B and PRD 49.

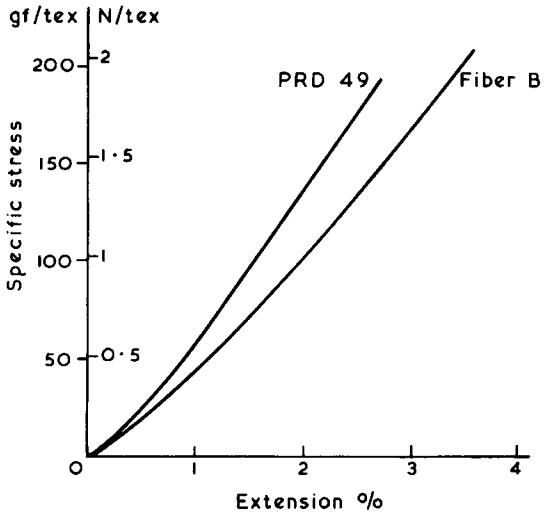

Fig. 3. Typical stress–strain curves of Fiber B and PRD 49.

The surfaces of untested filaments under the optical microscope and in the SEM show a generally smooth structure, but there are longitudinal splits in places, with many separated fibrils and ribbon-like fibrillar strands wound around the filament as shown in Figures 1(a), 1(b), 1(c), and 1(d). The existence of many fibrils and fibrillar strands separated from the outer layer of the filaments indicates a weak cohesion between fibrils. It is clearly necessary to take care in processing Kevlar in order to minimize the development of this type of damage. There is also evidence of slightly bulging lines around the surface located at various places along the filament, as shown in Figure 1(f) and 1(g). Dark lines of two different intensities may be seen when viewed in polarized light under

the optical microscope; they are located at various angles between +45° and −45° to the filament cross-sectional plane [Fig. 1(e)].

The high orientation of the filaments was shown by the fact that their birefringence Δn was found to be 0.445. An x-ray diffraction picture (Fig. 2) confirms the high crystallinity and orientation.

Simple Tensile Tests

Simple tensile tests were carried out on the Instron tester with a cross-head speed of 5 cm/min and a gauge length of 5 cm. The tests produced in both materials a very high breaking load and low breaking extension.

The load–extension curves of PRD 49 and Fiber B show a rapid rise up to the breaking point (Fig. 3); there is no yield region such as is characteristic of most polymer fibers. The tenacity of Fiber B and PRD 49 is more than twice as high as that of polyester tire filaments and superhigh-tenacity nylon and more than three times as high as that of medium-tenacity nylon. The initial tensile modulus of Fiber B is approximately 15 times that of medium-tenacity nylon and six times higher than that of polyester. The initial modulus of PRD 49 is approximately 20 times higher than that of medium-tenacity nylon and seven times higher than that of polyester. The above comparison is based on the values from Figure 3 and Shirley Institute data.[8]

TABLE I
Tensile Properties of Fiber B and PRD 49

	Fiber B	PRD 49
Diameter, measured in optical microscope, μm	12.4	12.4
Linear density, calculated, tex(den)	0.179(1.61)	0.180(1.62)
Instron Tests:		
Number of tests	24	20
Mean breaking load, N(gf)	0.361(36.8)	0.341(34.8)
Standard deviation, N(gf)	0.041(4.1)	0.068(6.9)
Variation coefficient, %	11.2	19.9
Max. value, N(gf)	0.422(43)	0.569(58)
Min. value, N(gf)	0.275(28)	0.196(20)
Tenacity, N/tex(gf/tex)(gf/den)	2.015(205.4)(22.9)	1.894(193.0)(21.5)
Standard deviation, N/tex (gf/tex)(gf/den)	0.226(23.1)(2.6)	0.377(38.4)(4.3)
Max. value, N/tex (gf/tex)(gf/den)	2.35(240)(26.7)	3.16(322)(35.8)
Min. value, N/tex (gf/tex)(gf/den)	1.53(156)(17.4)	1.09(111)(12.4)
Breaking extension, %	3.67	2.77
Standard deviation, %	0.45	0.25
Variation coefficient, %	12.2	9.2
Max. value, %	4.60	3.20
Min. value, %	3.00	2.30
Mean breaking secant tensile modulas, N/tex (gf/tex)(gf/den)	55.3(5635)(626)	69.0(7038)(782)
Standard deviation, N/tex (gf/tex)(gf/den)	4.63(472)(524)	17.7(1804)(200)
Variation coefficient, %	8.4	25.6
Initial tensile modulus from stress–strain curve, N/tex (gf/tex)(gf/den)	38.4(3900)(433)	427(4250)(472)

Table I summarizes mean values and other statistical characteristics of the results in the simple tensile tests made on Fiber B and PRD 49. Fiber B shows approximately the same irregularity in breaking load and breaking extension. The irregularity of extension in PRD 49 is similar to that in Fiber B, but the irregularity of breaking load is twice as high. It may be noted that the maximum strength value for PRD 49 was greater than that of Fiber B.

These test results should not be regarded as more than indicative of the fiber properties: a much more extensive statistical survey would be needed to obtain definitive results. Furthermore, in a material of such high stiffness, there may be errors due to softness of the measuring system, with a consequent underestimate of modulus and overestimate of breaking extension.

Fracture Morphology of Simple Tensile Failure

After tensile failure on the Instron tester, we examined the samples using the optical microscope and the SEM. All examined samples show a very long fracture with extensive splitting in a longitudinal direction. The optical microscope views show that the fracture occurs by prolonged axial splitting, but little detail is visible. In order to get complete views of the breaks at a reasonable magnification it is necessary to make montages of about ten SEM pictures. These are difficult to reproduce. SEM views of simple tensile fracture of the Fiber B filament are shown in Figure 4. Long montages of both broken ends are supplemented by some sections at higher magnification. The appearance is typical of both Fiber B and PRD 49. The fracture appears to develop along a plane at a very small angle to the filament axis. The length of fractures varies between approximately 500 and 800 μm (40 to 70 filament diameters). As the diameter of a filament is about 12 μm, the angle between the plane of the fracture and the filament axis must average about 1° to 1.5°.

The two broken ends usually differ in appearance: one end shows extensive splitting [Fig. 4(b)], while the other is a single, solid piece [Fig. 4(a)]. The "solid" end has split off from the other end and tapers in an elliptical cross section from the full filament cross section, where the split starts, to a small tip. In the other portion, there are many tips from separate splits which run back to two or more major splits at the beginning of the failed region. This splitting is usually accompanied by loose fibrillar bundles projecting from the surface of the fracture in several directions. A more recent series of tests by B. Lomas shows that there is no correlation between the direction of these ends and the direction of extrusion or winding on the package. Out of a total of 20 tests, the solid end was on the piece nearer the surface of the package in eight specimens and on the piece nearer the center of the package in another eight specimens; one specimen showed V-shaped ends, and three had both ends solid without multiple splits.

A possible mechanism of fracture development is shown schematically in Figure 5. An imperfection on the surface of the filament [such as shown in Fig. 1(d)] may act as the initiation point in the breakup of the fibrillar unit under the increasing load. The longitudinal shear stresses, induced at the root of the initial gap, cause longitudinal splitting of the first bundle of fibrils. There are also tensile stresses acting around the root. The tensile modulus and strength are much higher than shear modulus and strength; therefore, the crack develops under the above-mentioned steep angle. After the next layer of fibrils has

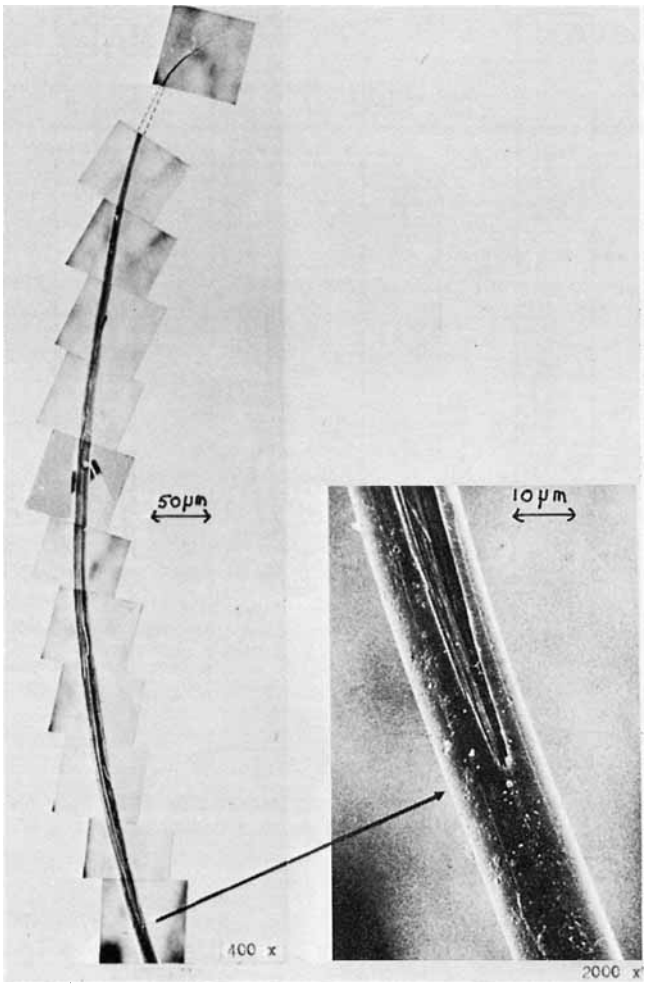

(a)

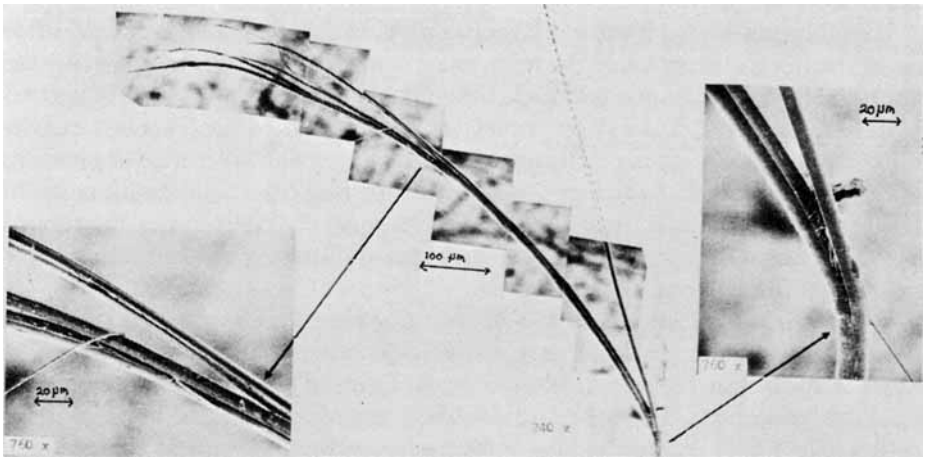

(b)

Fig. 4. Fiber B simple tensile fracture: (a), (b) SEM montages of opposite ends with some sections at higher magnification (breaking strength 42 gf, breaking extension 4.4%).

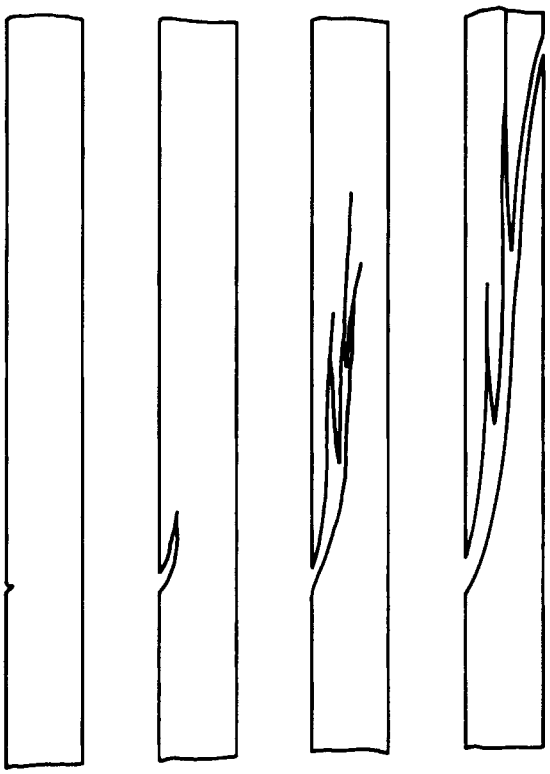

Fig. 5. Schematic representation of simple tensile fracture development in Fiber B and PRD 49. Note the transverse dimensions are expanded for clarity; actual breaks extend over longer lengths relative to filament diameter.

broken, a new gap is opened up, and there is again a concentration of shear stresses at the new root which results in splitting the next layer of fibrils. Likewise, the break is transmitted from one fibrillar unit to the next until the filament is broken completely.

It may be noted that if the crack propagation, with splitting, is in one direction along the fiber, and provided the main crack continues to propagate at a rate not appreciably less than the other cracks, then this main crack must reach the other surface first: thus, it is not surprising to find one end as a solid piece and the other with multiple cracks. The only conditions in which both ends would show multiple splits would be *either* if separate branching cracks propagating in opposite directions joined up *or* if the main crack (to the right in Fig. 5) stopped while the branches grew: and both these possibilities would lead to forms of splitting different from that observed.

When the whole lengths of the broken samples were examined, we found (under the optical microscope and in the SEM) bulging lines located some distance from the fractured end. Two different forms of these lines were observed: distinct dislocations [Fig. 6(a)] and double dislocations giving a "bow" configuration [Fig. 6(c)]. These bulging lines could occur as a result of compression forces developed in the filament during the snap-back after break. Possibly, there might be a relationship between the slightly bulging lines in untested filaments and the more pronounced bulging lines after break. If we compare

the spacing between dark lines observed in untested filaments under the optical microscope with the spacing of bulging lines in Figure 6(b) (optical micrograph) and Figure 6(a) (SEM micrograph), we can see that it is approximately the same.

The partially broken, sharply bent, split sections of the filament and transverse bands located just below the bend in the fracture region [Fig. 6(d)] may be seen

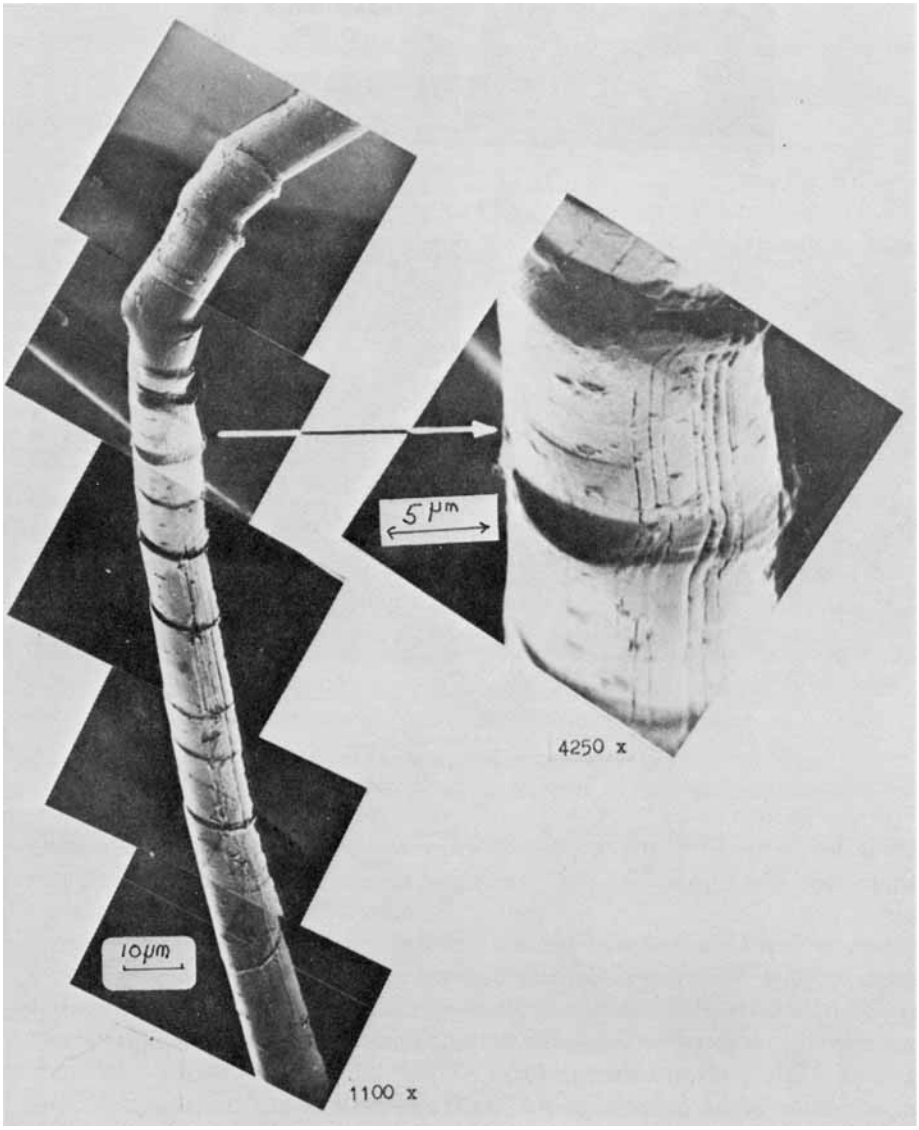

(a)

Fig. 6. SEM and optical views of various types of structural dislocations—"bulging lines"—discovered at some distance back from ends of tensile fracture: (a) SEM micrographs showing "ring-like" bulging lines in Fiber B. (b) Optical micrograph showing bulging lines in Fiber B. (c) SEM micrograph presenting "bow" configuration bulging lines in PRD 49. (d) SEM micrograph of sharply bent, split sections of PRD 49 filament with distinct transverse bands located just below the bend in the fractured region.

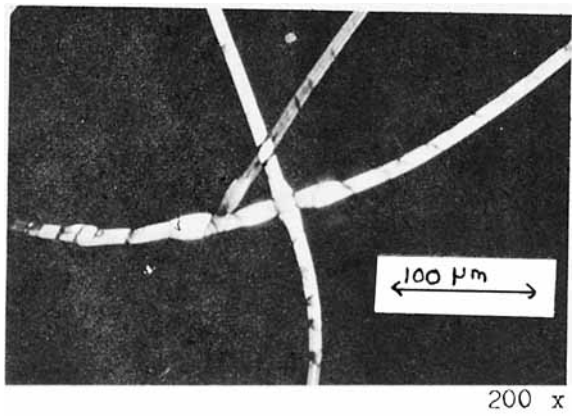

(b)

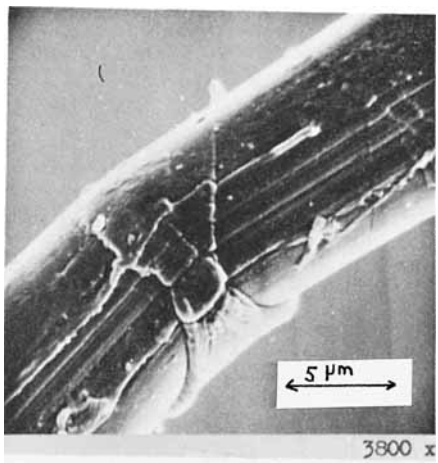

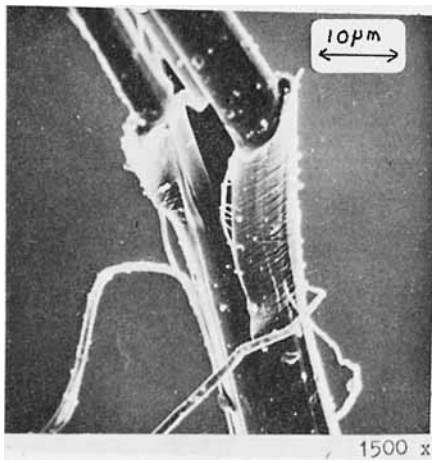

(c) (d)

Fig. 6. (*continued from previous page*)

as additional evidence of the compression forces. Another remarkable example of snap-back of a ribbon-like fibrillar strand into opposed helices is shown in Figure 7.

Figure 8 shows the internal surfaces of the split sections within a tensile fracture of Fiber B filament. Comparing internal surfaces with the outer surface of the filament, the difference may be clearly seen: internal surfaces exhibit transverse lines with periodically repeated spacing approximately 0.5 μm, while an outer surface is smooth and uniform. We propose that these lines are characteristic of the internal structure of Fiber B and PRD 49 and do not appear only after a tensile break. This assumption might be confirmed by closer examination of an internal surface of peeled filaments (thicker than those we had obtained) before any tests.

In the fiber fracture classification given by Hearle,[9,10] there is a group called "fracture with axial splitting." Tensile fracture of Fiber B and PRD 49 could be included in that group, showing extensive axial splitting approximately 70 times longer than a filament diameter.

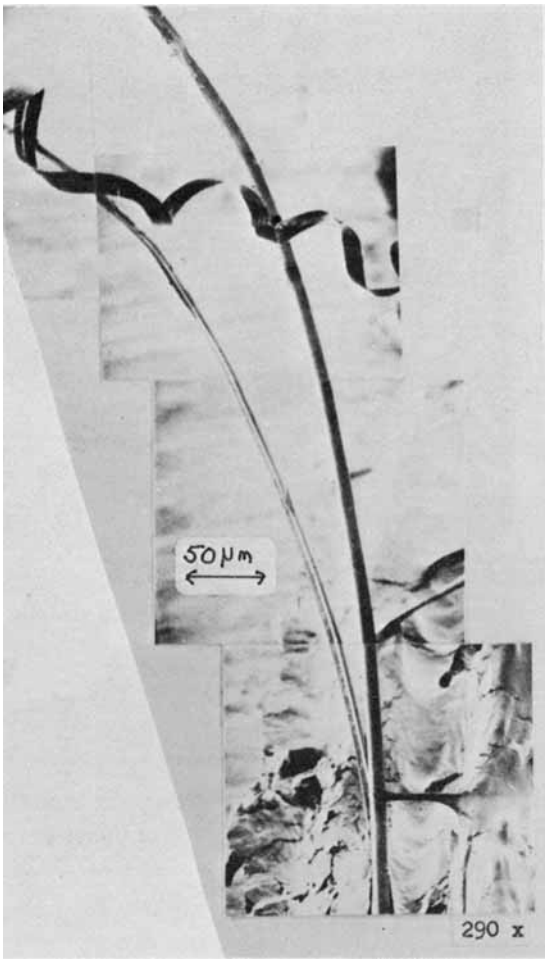

Fig. 7. SEM micrograph of PRD 49 tensile fracture, showing effects of snap-back on a ribbon-like fibrillar strand which has separated from the filament.

A fracture of Fiber B in liquid nitrogen also shows break by axial splitting, with very marked transverse lines in the internal surface (Fig. 9). Fiber B exhibited an extremely high breaking strength in liquid nitrogen and on extensibility much lower than at room temperature.

FATIGUE TESTS

Test Method

A study of fatigue properties of Fiber B and PRD 49 was carried out on Bunsell's fatigue tester, of which a detailed description has been given elsewhere.[7]

A working gauge length of 40 mm was chosen for our experiments. The sample was subjected to a load cycling with a maximum load in each cycle lower than the breaking load of the material in a simple tensile test. The cycling frequency was 50 Hz. The working speed of the upper-jaw vertical movement from the motor through the gears was 1.3 cm/min.

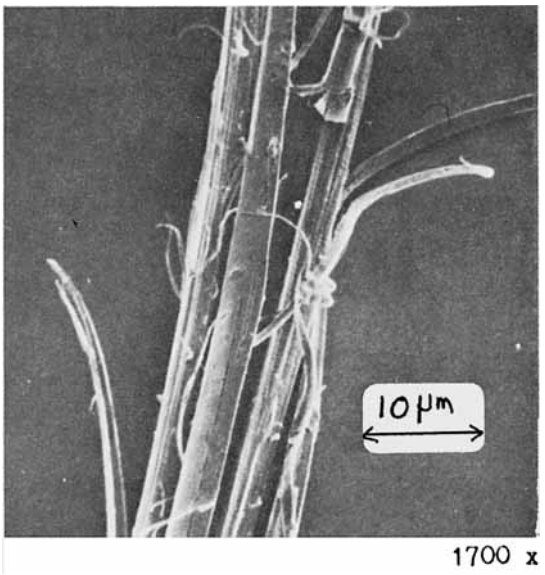

Fig. 8. Internal transverse lines in the tensile fractured region of Fiber B.

On starting the experiment, the motor stretches the sample until the selected maximum load is reached. An oscillatory load amplitude is being set up during the initial period.

After the initial period the lower jaw vibrates sinusoidally with the set amplitude, and the filament undergoes periodical or quasi-periodical loading with the load P varying within the interval:

$$\max(P_{\text{mean}} - P_{\text{osc}}; 0) < P < P_{\text{max}}$$

where $P_{\text{mean}} = 1/\text{T} \int_t^{t+\text{T}} P\,dt$ is the mean load; $P_{\text{osc}} = (P_{\text{max}} - P_{\text{mean}})$ is oscillatory load; P_{max} is maximum load; t is time; and T is period.

Different load conditions which may take place are schematically illustrated in Figure 10. The real signal corresponding to the applied load is observed on the oscilloscope. The apparatus was designed in such a manner that whenever, during the test, the maximum load on the sample drops below a required value, the motor switches on to compensate it by stretching the sample.

The behavior of Fiber B and PRD 49 during the fatigue test was different from that of nylon and other fibers. Nylon and other textile fibers display a certain amount of viscous flow (or plastic deformation) which results in progressive stretching of the fiber during the whole period of the fatigue test in order to maintain the set maximum load. By contrast, Fiber B and PRD 49 appear to behave during the fatigue test like perfectly elastic springs. After producing the required maximum load at the beginning of the test, the motor stops and the sample length and mean load remain constant. After a period of vibration, the filament breaks and there is only a small inertial movement of the upper jaw at the moment of final filament break.

In general, the filaments during the fatigue test were repeatedly copying relevant parts of the steep stress–strain curves from the Instron, and, correspondingly, the amplitudes of the lower jaw had to be set to less than 0.5 mm.

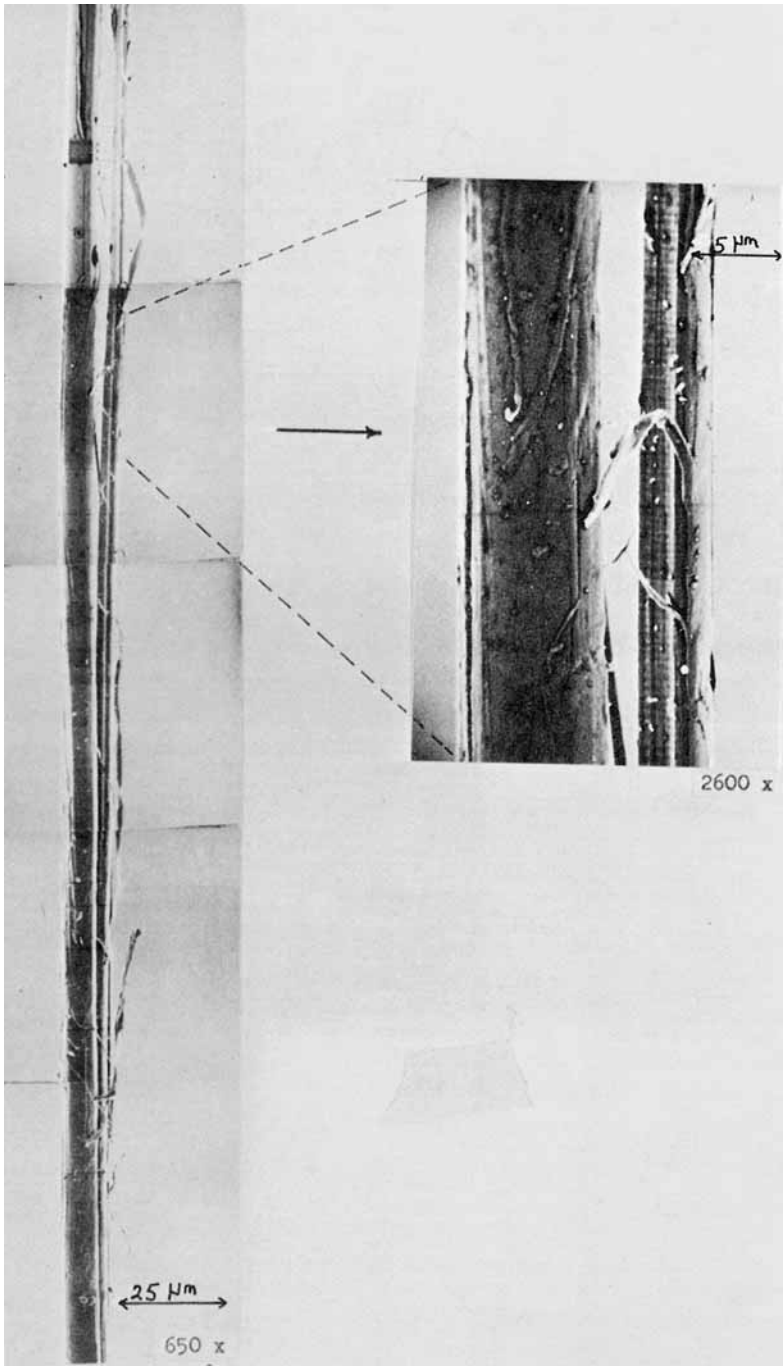

Fig. 9. SEM micrographs showing tensile fracture of Fiber B in liquid nitrogen, with separate section at higher magnification.

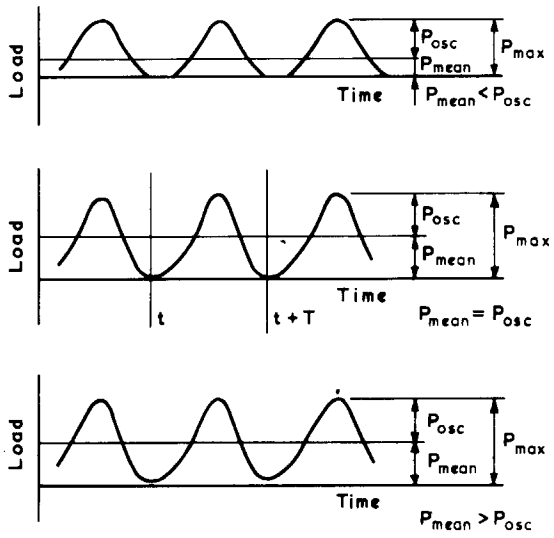

Fig. 10. Different loading conditions of fatigue testing.

The static extension observed was about 2–3%, depending on the set maximum load.

Some possible outcomes of the fatigue tests may be as follows: (a) break during the initial period (i.e., before or just after reaching the chosen maximum load); (b) break after a certain number of cycles (i.e., after a minimum of 9000 cycles under set loading conditions); (c) absence of a break at the chosen testing period.

Only samples broken in the middle are taken into account; breaks near the

TABLE II
Summary of Results of Fatigue Tests of Fiber B and PRD 49

	Fiber B				PRD 49			
Test no.	Oscillatory load, gf	Mean load, gf	Maximum load, gf	Life time, no. of cycles	Oscillatory load, gf	Mean load, gf	Maximum load, gf	Life time, no. of cycles
1	11	9	20	immediate break	12	9	21	1.8×10^5
2	12	10	22	0.15×10^5	14	10	24	immediate break
3	12	10	22	0.51×10^5	12.5	12	24.5	0.45×10^5
4	13	12	25	not broken after 30.75×10^5	13	12	25	0.62×10^5
5	14	12	26	0.09×10^5	13	12	25	9.10×10^5
6	13.5	13	26.5	not broken after 162.2×10^5	12	14	26	immediate break
7	14.5	13.5	28	2.85×10^5	13	14	27	0.62×10^5
8	14.5	14	28.5	0.09×10^5	14.5	12.5	27	2.40×10^5
9	15.5	13	28.5	8.77×10^5	14	13	27	4.05×10^5
10	15	14	29	immediate break	14	13	27	7.80×10^5
11	15	14	29	immediate break	14.5	14	28.5	0.75×10^5
12	15	14	29	0.08×10^5	15	14	29	immediate break
13	12	17	29	6.57×10^5	15	14	29	immediate break
14	15	14	29	21.90×10^5	15	14.5	29.5	immediate break
15	15.5	14	29.5	9.75×10^5	18	16	34	immediate break
16	15.5	14.5	30	0.27×10^5				
17	16	15	31	immediate break				
18	16	15	31	immediate break				
19	16	15	31	0.27×10^5				
20	16.5	15.5	32	0.09×10^5				
21	17.5	17	34.5	2.30×10^5				

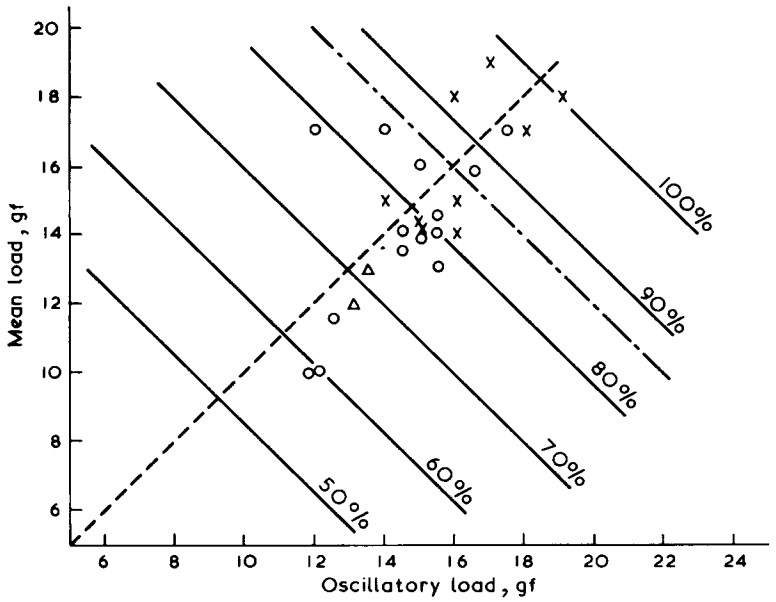

Fig. 11. Results of Fiber B fatigue tests in relation to various chosen values of mean load and oscillatory load: (O) fatigue failure; (x) immediate failure; (Δ) not broken; (—) lines of equal maximum load (% of Instron breaking load); (— - —) mean maximum load of immediate failures; (- - -) line of zero minimum load.

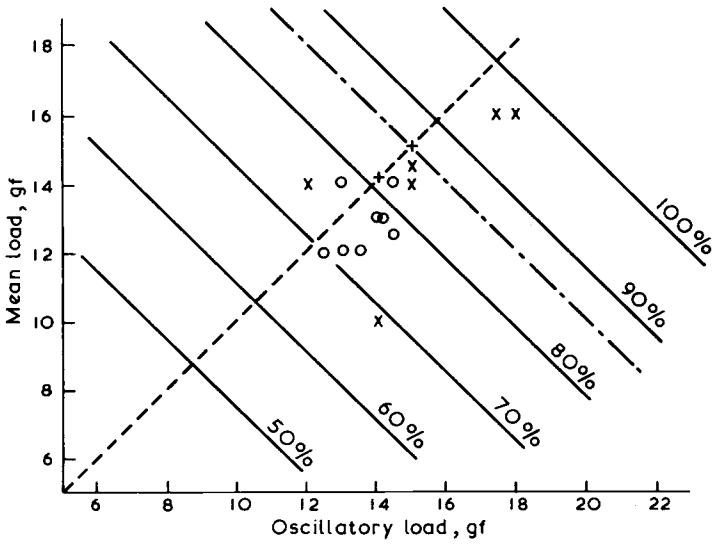

Fig. 12. Results of PRD 49 fatigue tests in relation to various chosen values of mean load and oscillatory load (symbols as in Fig. 11).

jaws are discarded. The summary of the results of fatigue tests of Fiber B and PRD 49 is shown in Table II. These data are shown in Figures 11 and 12 in relation to various chosen values of mean load P_{mean} and oscillatory load P_{osc}. The broken line shown in these figures divides the plane into upper left segment with $P_{mean} > P_{osc}$ and lower right segment with $P_{mean} < P_{osc}$. Perpendicular

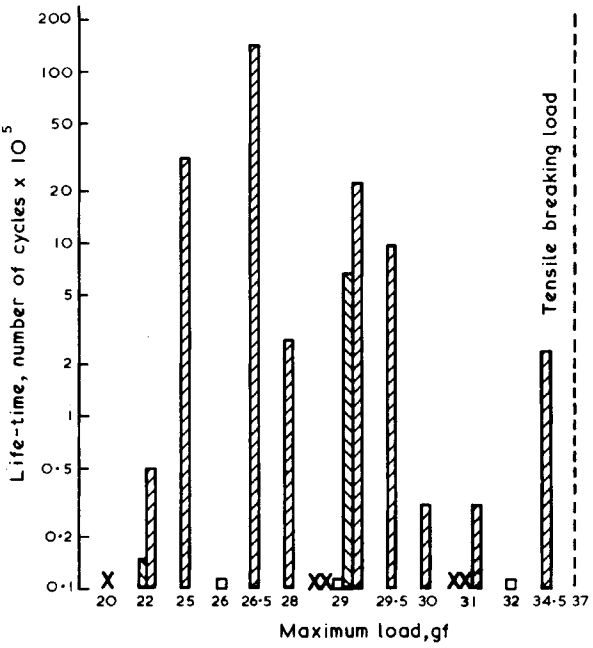

Fig. 13. Diagram of Fiber B fatigue lifetime: (x) immediate break; (—) lifetime 0.1×10^5 cycles; blocks show individual results with lifetime 0.1×10^5 cycles.

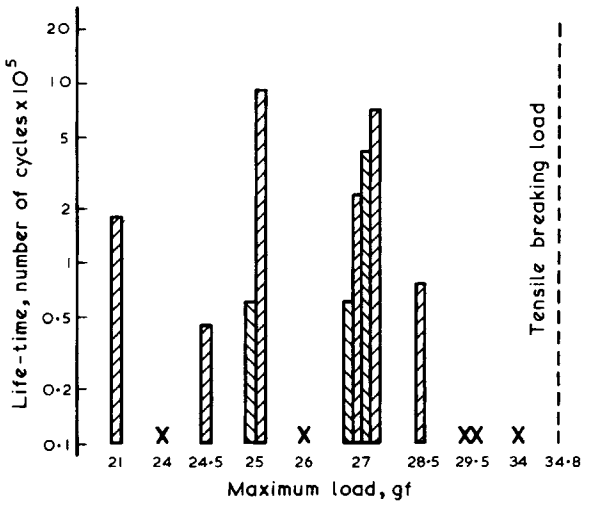

Fig. 14. Diagram of PRD 49 fatigue lifetime (symbols as in Fig. 13).

to the broken line in each figure are the lines of equal maximum load $P_{max} = P_{mean} + P_{osc}$ corresponding to 100%, 90%, ... 50% of the mean value of the breaking load in simple tensile tests.

As may be seen in Figure 12, all the five samples of PRD 49 subjected to a maximum load larger than 82% of mean breaking load and also three samples below 82% have broken during the initial period. Something in the method of mounting or application of load in the apparatus, thus, seems to lead to a lower

TABLE III
Results of fatigue tests using different procedures

Tensile breaking load, gf	Max. load in Fatigue test, gf	Tensile breaking load, %	Life time, no. of cycles × 10^5
34	22 (normal speed)	65	0.51
30	slow increase 18–24 (normal speed)	77	7.2
30	22–29 (movement by hand)	100	11.7

breaking load. All the other samples of PRD 49 under maximum load of less than 82% have broken after various periods of cycling.

In the case of Fiber B (Fig. 11), the nine breakages during the initial period are dispersed between 80.5% and 100% of the mean breaking load, and the 14 fatigue breakages, between 60.5 and 90.4%. The two samples tested under maximum loads of 69.5% and 73.5% (of the mean breaking load) survived 17 and 79 hr of cycling, respectively. The dispersion of the experimental results may be seen as reflecting a high irregularity of the tensile properties of the materials.

Although the results are considerably scattered and do not show the distinct areas of the three above-mentioned outcomes as clearly as in the case of nylon 66,[11] it may be concluded that the breaking resistance of the filaments of both types (Fiber B and PRD 49) is to a limited degree adversely affected by cycling.

The performance of Fiber B under our fatigue testing seems to be better and the rate of deterioration of mechanical properties lower than that of PRD 49. This conclusion is supported by comparing the lifetime (Figs. 13 and 14), which is higher for Fiber B than for PRD 49. The experimental values, however, are very uneven, and especially striking is the apparent absence of correlation between the lifetime of the samples and the set maximum load.

As a matter of interest, we carried out fatigue tests on three filaments of Fiber B using the following different procedures: (a) quick application of maximum load at normal speed of extension during about 1 min; (b) gradual increase of maximum load during the period of a few hours, each increase being made at the normal speed of extension; (c) slow increase of maximum load by hand operation. Tensile tests were also performed on other portions of each filament. The results of these tests are shown in Table III. These tests show that while in the first test the applied maximum load was 70% of the breaking load, in the second and third tests filaments seem to become stronger during the load cycling, and we were able to increase the maximum load up to 77% and 100% of the breaking load, respectively. This is an interesting finding but it should be supported by further testing.

Fracture Morphology of Fatigue Failure

All the filaments broken in fatigue tests were examined under the optical microscope, and a few of them were subjected to a detailed investigation in the SEM. We could not identify in Fiber B and PRD 49 such a basic difference

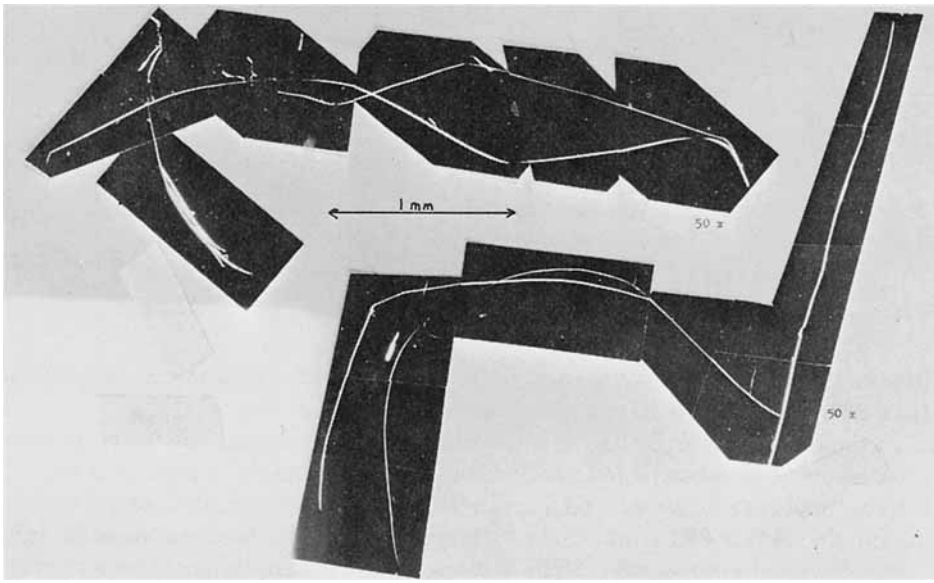

Fig. 15. (a), (b) Montages of Fiber B fatigue fracture (both broken ends) taken under the optical microscope (failed after 2.85×10^5 cycles at max. load = 28 gf).

between the fracture morphology of simple tensile failure and fatigue failure as we did in nylon 66 and other textile fibers.[11,12] This finding seems to agree with the absence of plastic deformation during the fatigue test as shown in the previous chapter. The fact that the filament behaves during the fatigue test as a nearly perfect spring implies little change of mechanical properties in the longitudinal direction. Consequently, little difference between the fracture patterns in tensile and fatigue tests was to be expected.

On the other hand, all the filament failures following the cycling on the fatigue tester occurred under a maximum load which was lower than the average breaking load in a simple tensile test. Our investigation of the fatigue-broken filaments was aimed to reveal possible structural causes and signs of the deterioration of breaking resistance during cycling.

The most remarkable difference between tensile and fatigue-broken filaments is in the much deeper and longer splits occurring in fatigue breaks compared with normal tensile breaks; in addition, this longitudinal splitting is much more extensive and appears often at both broken ends. This may be seen as a consequence of loosening the comparatively weak interfibrillar bonds during the high-frequency loading and unloading.

Figures 15(a) and (b) show montages, taken through the optical microscope, which illustrate the fatigue failure (both broken ends) of Fiber B. The fracture extends over a total length approximately of 6 mm (485 times the fiber diameter), which is about seven times longer than in a simple tensile break. Sometimes, due to the extensive splitting of the filaments, portions of the fracture are lost. An example of this is shown in Figure 15(b) where the broken portion of the fiber lies across the fractured end. In this case, the broken part is still present, but in most cases losses of this kind are not discovered until the fracture is examined in the SEM.

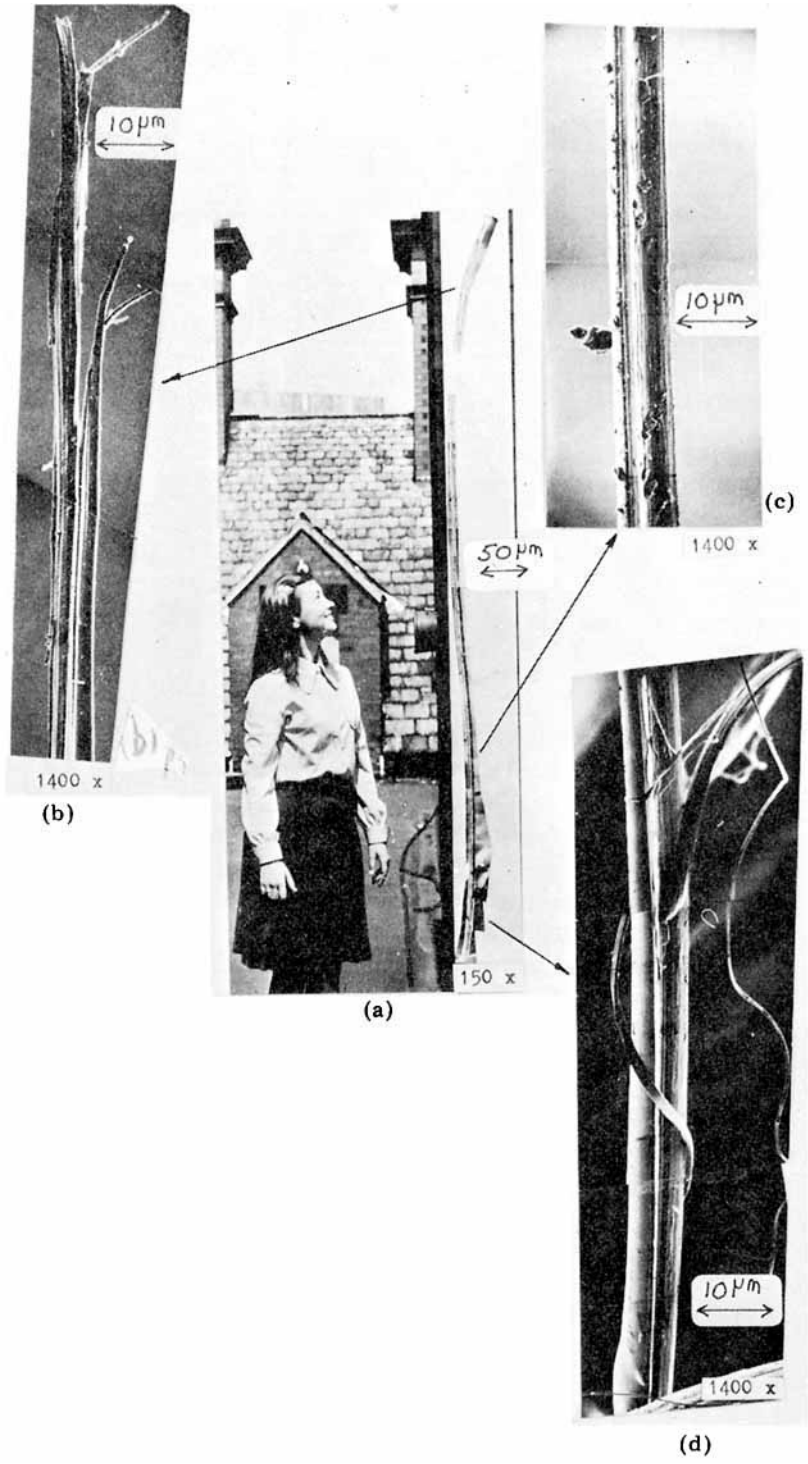

Fig. 16. Montage comparing the length of the Fiber B fatigue fracture with the human height, and SEM micrographs showing some sections of the fracture at higher magnification.

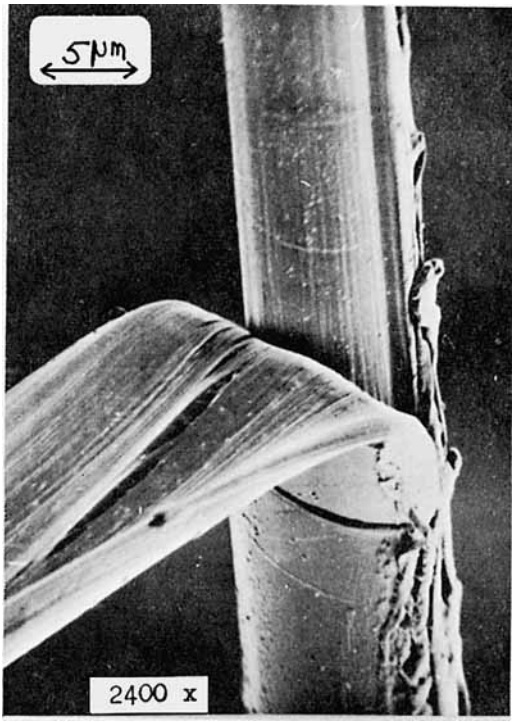

Fig. 17. SEM micrograph showing a section of PRD 49 fracture. Note a thin layer peeled from the main body and splits within this thin layer.

We also observed a similar type of fatigue fracture morphology in PRD 49. Because of the enormous length of the fracture, it was difficult to record as a whole in the SEM at magnifications high enough to detect fine details within the fracture surface. In some cases montages were made consisting of 25 or more different sections, but they still only covered part of the full-fracture length, and we often missed some sections; Figure 16(a) illustrates graphically the problems involved in making these montages.

Figure 16(b) illustrates the top section of a typical Fiber B fatigue fracture with multiple splits (this is only a part of a montage taken in the SEM in 27 stages). Figure 16(c) shows the inner surface of the same fracture (about 3 mm from the top) with transverse lines going along the whole length with about the same spacing as in a simple tensile break. In this illustration, the thickness of this split portion of the fracture represents only about half of the diameter of the filament. The shape of the cross section in this part of the fracture is semicircular with a reentrant portion in the middle of the inner surface. Figure 16(d) shows a part further from the broken end. In Figure 17, a thin layer peeling from the main body of a filament of PRD 49 can be seen; there are also splits within this thin layer. Another example of multiple splits in Fiber B occurring in the middle portion of the fatigue fracture, with many fibrillar bundles projecting from the inner surface, is shown in Figure 18.

The result of loosening the interfibrillar bonds due to cycling loading in PRD 49 is illustrated in Figure 19 where, in the middle portion of the fracture, the filament has broken into two distinct parts forming a hole in the filament re-

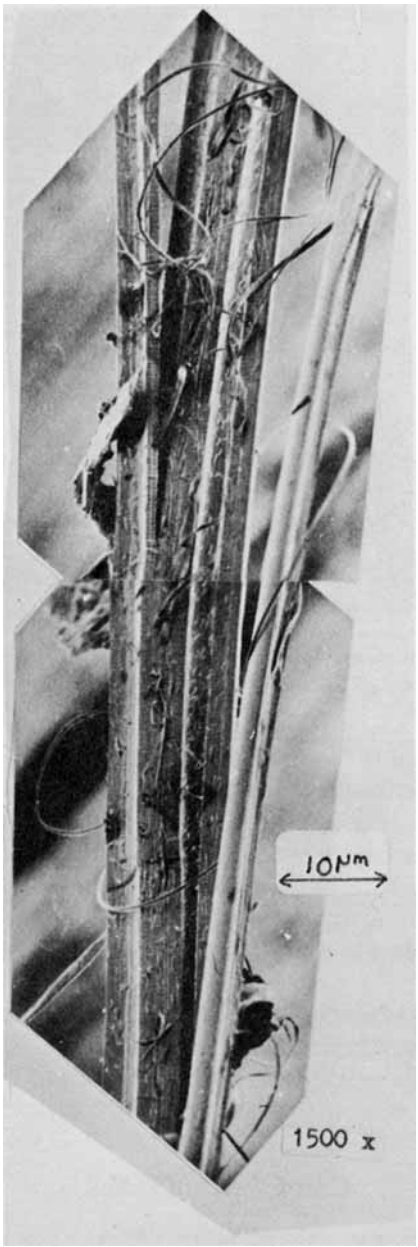

Fig. 18. SEM micrograph showing multiple splits in the middle portion of the Fiber B fatigue fracture.

sembling the eye of a needle. This unbroken split portion of the filament is an example of an earlier stage of development of the splits during the cycling (it is likely that most of the broken split portions went originally through that stage).

In fatigue-broken samples as in tensile ones, bulging lines (dislocations) were found some distance from the fracture during a detailed examination in the SEM; they were located at various angles to the filament axis [Fig. 20(a)]. Most of these

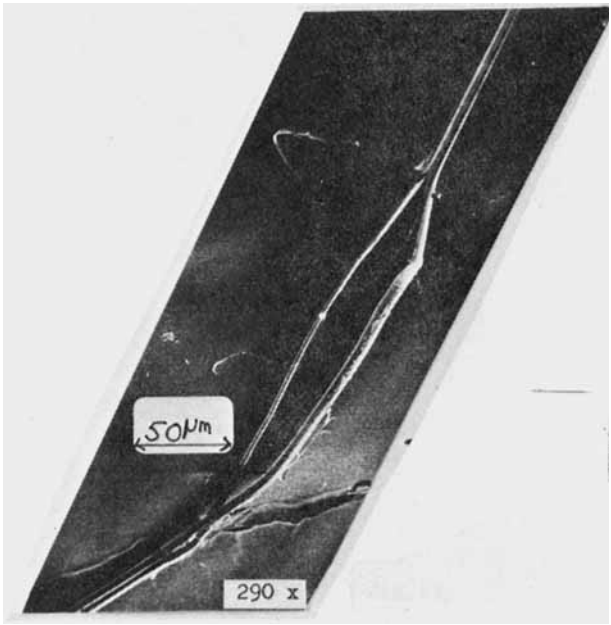

Fig. 19. SEM micrograph showing isolated split portion within the fractured region of PRD 49 fatigue failure.

bulging lines, in contrast to those observed in tensile broken filaments show many cracks extending from the lip of the bulge (dislocation) approximately parallel with the filament axis [Fig. 20(a) and (b)].

Distinct dislocations (sharp bends) were also often found in the middle of the split portion of the fracture, as illustrated in Figure 21(a) (PRD 49). A possible consequence of compression forces (as in tensile break) can be seen at closer investigation of this dislocation in Figure 21(b), which also shows closely spaced transverse lines.

The fatigue fracture morphology of Fiber B and PRD 49 could be included in the same group of fracture forms[9] as tensile fracture of these fibers, i.e., fracture with axial splitting, though this has been subdivided into tensile and fatigue groups.[10]

Creep Tests of Fiber B

Fiber B and PRD 49 as mentioned above did not show any appreciable plastic deformation or creep when tested on the fatigue tester during and up to 50 h or so. The absence of significant viscoelastic or plastic deformation was also observed when testing Fiber B under a steady load on the creep tester, whose description is given by Bunsell.[13]

Immediately after applying the load (8, 13, or 26.5 g), the filament stretched to the extent corresponding roughly to the stress–strain curve from the Instron. The extension remained almost constant for about 2 hr. During the next two to three days, we observed a barely noticeable additional extension of 0.1–0.2% in each of the three cases.

The small value of static creep as compared with total absence of dynamic creep might be explained by the fact that on the fatigue tester, the filament is

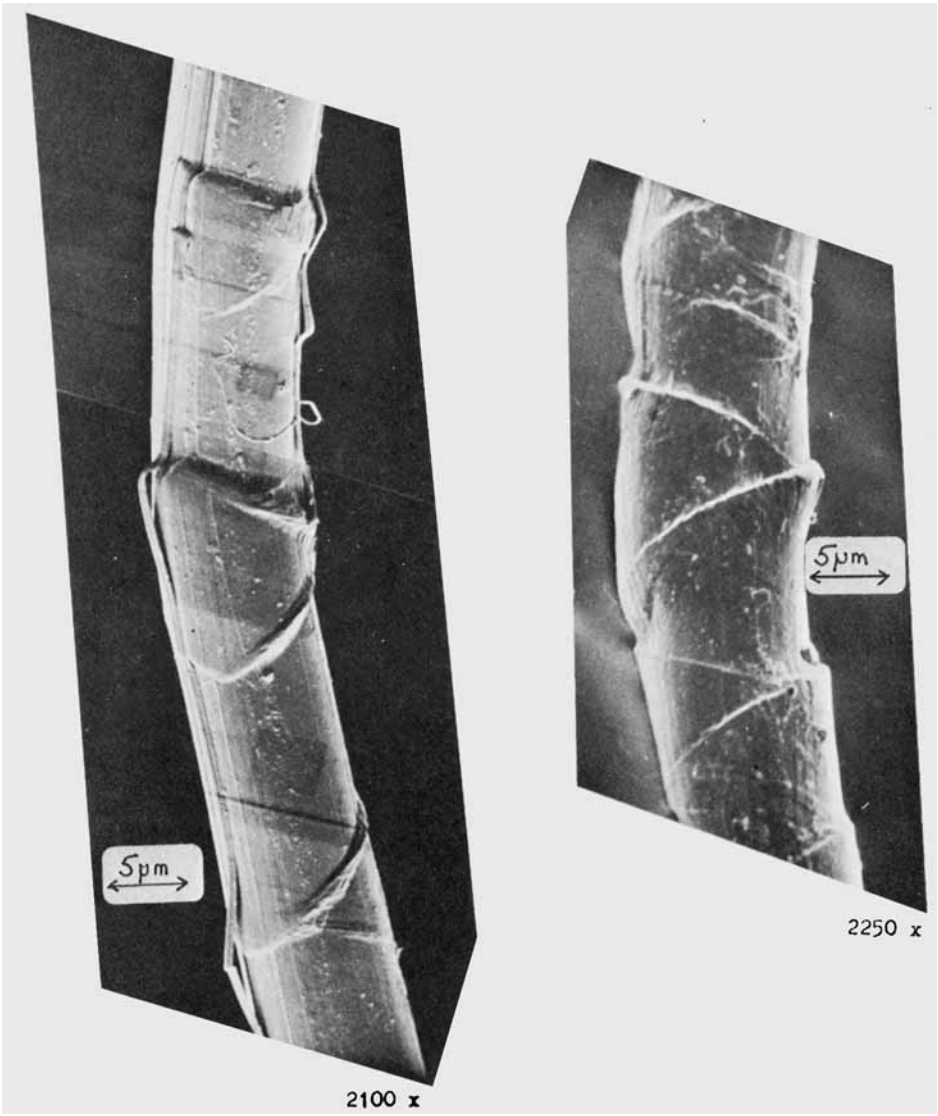

Fig. 20. (a), (b) SEM micrographs showing bulging lines at some distance from the fractured end of a Fiber B filament after fatigue failure. Longitudinal cracks are also apparent.

under a load near to the maximum only during a short interval in each cycle, after which it is allowed to relax. Our observation of dynamic and static creep, however, should not be taken as final and conclusive because of insufficient accuracy of the deformation readings on both fatigue tester and creep tester as measured against generally low deformability of the Fiber B and PRD 49.

CONCLUSIONS

The tests which we have made confirm the remarkably high stiffness and strength of Kevlar fibers. The fracture morphology shows, furthermore, that

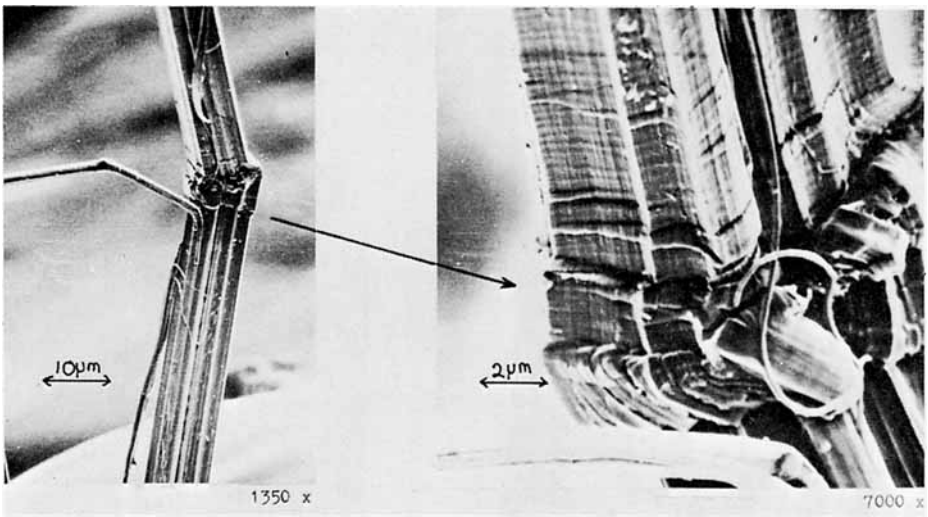

(a) (b)

Fig. 21. (a), (b) SEM views of dislocations within the fatigue fracture region of PRD 49 at different magnifications.

when failure comes, it is not the result of fracture across the axis of orientation but of splitting along the axis. This axial splitting will derive from any discontinuity, such as a surface flaw, which must give rise to shear stresses. The fact that there are no chain molecules crossing and supporting axial planes, but only weak intermolecular forces between these planes, will then lead to the axial splitting.

If the splitting, or multiple splitting, is even slightly off axis (by 1° or 2°), then it will eventually over long lengths cross the fiber and lead to a loss of continuity; before this happens, there may be a transverse failure of the small residual area of fibers which bear the whole load.

The easy axial splitting has also been shown in Kevlar fibers broken down by compressive forces in the x-press test.[14]

In addition to its theoretical interest, the fact that Kevlar breaks by axial splitting is also of great practical importance. Filaments are not used separately; they are part of a bundle in a multifilament yarn and, in many uses, contained within a matrix. Under these conditions, filaments which have split will still contribute greatly, throughout their length, to the load-bearing capacity of the assembly. The aspect ratio of the split fibrils is high and so they will be effective as "staple fibers." Kevlar in use is thus likely to be effectively stronger than would be expected from tests on single filaments.

This advantage will be even more marked in the even longer axial splits which result from fatigue tests. It is now a general experience of our tensile fatigue testing of fibers that even when tensile breaks occur transversely, fatigue breaks usually occur by axial splitting; and where tensile breaks show axial splitting, fatigue breaks are longer and more split. This applies also to Kevlar. However, the effects of tensile fatigue on reducing the load-bearing capacity of Kevlar appear to be quite small, little more than would be allowed for in variability of test data and hardly worthy of counting separately in determining safety factors.

In view of the considerable scatter of the results, and the range of possible combinations of load, it is difficult to make firm comparisons without carrying out very large numbers of tests. However, the following tentative conclusions seem justified in their application to the particular Fiber B and PRD 49 samples tested: (a) The method of application of load in the fatigue tester appears to lead to a breaking load which is lower than in an Instron tensile test. (b) The application of an oscillatory load does appear to cause a further small drop in the maximum load needed to cause failure; this effect appears to be more marked when the fiber is allowed to go slack. (c) Nevertheless, the fatigue effect is much less severe than in nylon or polyester fibers; allowing for the variability of results, it appears that the rated loading under fatigue conditions comparable to those used in these tests should be taken to be about 75% of the Instron breaking load or 90% of the load for immediate failure under these conditions. A comparable figure for the other synthetics would be around 60%.

The results presented in this paper, which concentrate on the failure morphology, are in general agreement with the studies of mechanical properties reported recently by Bunsell.[15]

This work has been carried out with support from Procurement Executive, Ministry of Defence. The authors also acknowledge the help of E.I. du Pont de Nemours & Co., Inc., in supplying yarn samples and of Miss B. Lomas (U.M.I.S.T., Manchester) for useful discussions.

References

1. *Text. Inst. Ind.*, **12**, 380 (1974).
2. W. B. Black and J. Preston, High-modulus wholly aromatic fibers, M. Dekker, INC., New York, 1973, p. 5.
3. C. B. Chapman, *Fibres*, Butterworth, London, 1974, pp. 80–81.
4. R. Meredith, *Text. Progr.*, **7** (No. 4), (1975).
5. J. W. Rothuizen, *Text. Inst. Ind.*, **11**, 142 (1973).
6. du Pont de Nemours & Co., *Information Bulletins No. 4, 5, 6, 7*, 1974.
7. A. R. Bunsell, J. W. S. Hearle, and E. Hunter, *J. Phys. Ed.*, **4**, 868 (1971).
8. *Fibre Data Summaries*, Shirley Institute, Manchester, July 1966.
9. J. W. S. Hearle, B. Lomas, and A. R. Bunsell, *Appl. Polym. Symp.*, **23** 147 (1974).
10. J. W. S. Hearle, in *Contributions of Science to the Development of the Textile Industry*, M. Cordelier and P. W. Harrison, Eds. Textile Institute and Institut Textil de France, 1975.
11. A. R. Bunsell and J. W. S. Hearle, *J. Mater. Sci.*, **6**, 1303 (1971).
12. A. R. Bunsell and J. W. S. Hearle, *J. Appl. Polym. Sci.*, **18**, 267, 1974.
13. A. R. Bunsell, Ph.D. dissertation, Univ. Manchester Inst. Sci. Technol., 1972.
14. J. W. S. Hearle and S. C. Simmens, *Polymer*, **14**, 273 (1973).
15. A. R. Bunsell, *J. Mater. Sci.*, **10**, 1300 (1975).

Received June 11, 1976